Molecular Catalysis 580 (2025) 115134

Contents lists available at ScienceDirect

Molecular Catalysis

journal homepage: www.journals.elsevier.com/molecular-catalysis

Exploring the hydrodeoxygenation of lignin β-O-4 dimer model compound and bio-oil by DFT and experimental studies

Yanjun Wen [a,*], Foteini Zormpa [a], Dmitry I. Sharapa [a], Felix Studt [a,b], Klaus Raffelt [a,*], Nicolaus Dahmen [a]

[a] Institute of Catalysis Research and Technology, Karlsruhe Institute of Technology (KIT), Hermann-von-Helmholtz-Platz 1, 76344 Eggenstein-Leopoldshafen, Germany
[b] Institute for Chemical Technology and Polymer Chemistry, Karlsruhe Institute of Technology (KIT), Engesserstr. 20, 76131 Karlsruhe, Germany

ARTICLE INFO

Keywords:
Hydrodeoxygenation
Ru catalyst
Lignin
Bio-oil upgrading
DFT calculations

ABSTRACT

Hydrodeoxygenation (HDO) is a pivotal process in the efficient utilization of biomass, with ruthenium (Ru) emerging as a highly effective catalyst for this reaction. A dimer model compound, more representative of bio-oil oligomers than monomers, was used to explore the HDO mechanism over a Ru catalyst through both density functional theory (DFT) calculations and experimental studies. Initially, the adsorption of 2-Phenylethyl phenyl ether (PPE) was examined through DFT, leading to the determination of an optimized structure. Subsequent calculations of the HDO reaction pathways on the Ru (0001) surface revealed that the β-O-4 linkage cleavage occurred with significantly low activation energy. For the experimental study, a Ru/Nb_2O_5 catalyst was synthesized using wet impregnation method. Characterization of this catalyst through scanning electron microscopy (SEM) and X-ray diffraction (XRD) confirmed its congruence with the DFT model. The catalytic performance of Ru/Nb_2O_5 was evaluated in the PPE HDO process, where it demonstrated high efficiency. The applicability of the Ru/Nb_2O_5 catalyst was extended to a real lignin bio-oil so as to further assess its effectiveness. This research provides a systematic study on PPE HDO over a Ru catalyst, illustrating the potential of using dimer model compounds in HDO mechanism investigations and the promising capabilities of Ru-based catalysts.

1. Introduction

Biomass resources represent the only renewable carbon resource in nature, and their rational utilization is of significant importance for global carbon emission control [1]. Regrettably, due to the high polymerization of lignocellulose, a major constituent of biomass, its efficient utilization poses a significant challenge. Biomass utilization encompasses a wide range of pathways, including biochemical processes such as fermentation, thermochemical methods like gasification and pyrolysis, and catalytic upgrading techniques [2–4]. Among these, fast pyrolysis has been extensively studied for their potential to produce bio-oil which can serve as intermediates for high-value fuels and chemicals [4–6]. However, the high oxygen content of bio-oil leads to several drawbacks: it is acidic and corrosive, has a low calorific value, and poor stability. These factors result in significant differences in properties compared to traditional fossil fuels, making direct utilization challenging. Consequently, hydrodeoxygenation (HDO) emerges as a promising industrial-scale technology for bio-oil upgrading.

Bio-oil primarily comprises water, organic monomers, and oligomers derived from the depolymerization of biomass macromolecules [7]. Currently, research on HDO predominantly focus on monomeric arenes, including compounds like phenol, guaiacol, vanillin, and others [8–11]. However, it is important to note that oligomers also play a crucial role in the composition and properties of bio-oil. Notably, oligomers mainly originating from incomplete lignin decomposition contribute to the high viscosity and the propensity for char formation during the upgrading and storage processes of bio-oil. Consequently, investigating the behavior of oligomers in the HDO process of bio-oil is essential. In the context of lignin polymer, the most relevant chemical bonds include β-O-4 (43–65 %), α-O-4 (4–8 %), and 4-O-5(4–7 %), among others (**Figure S1**) [12,13]. Of these, the β-O-4 linkage is the most prevalent, constituting over 40 % of lignin fraction in both softwood and hardwood [14]. Therefore, a model compound containing the β-O-4 linkage, such as 2-Phenylethyl phenyl ether (PPE), represents a good choice for studying the behavior of oligomers during HDO.

Density Functional Theory (DFT) serves as a robust tool for

* Corresponding authors.
E-mail addresses: wen.yanjun@kit.edu (Y. Wen), klaus.raffelt@kit.edu (K. Raffelt).

https://doi.org/10.1016/j.mcat.2025.115134

Available online 16 April 2025

investigating reaction pathways, predicting product distributions, and quantifying properties related to catalyst activity. During the recent years, DFT research is mainly focusing on the cleavage of $C_{aromatic}$-O bonds by aromatic monomers, leaving the study of the β-O-4 dimer model compound relatively underexplored. López and Li [15], studied the adsorption structures and potential reaction pathways of β-O-4 linkage molecules on the Ni (111) surface. They confirmed that the groups attached to the α-carbon and β-carbon, along with their spatial positioning, significantly influence the reaction barrier and the distribution of intermediates and products. Su and colleagues [16], investigated the reaction behavior of β-O-4 molecules on both $NbOPO_4$ and Pd clusters. They elucidated that the strong adsorption interaction at the Nb adsorption sites with oxygen plays a crucial role in facilitating the cleavage of the β-O-4 linkage, and they also endeavored to reveal the synergistic effect between the Pd cluster and $NbPO_4$ support.

In experimental studies, numerous researchers have utilized HDO of model compounds to test catalyst performance and investigate mechanisms. PPE is a prototypical model compound for studying β-O-4 linkage cleavage. Zhao and Luo [17], explored the kinetics and mechanisms of the PPE HDO reaction using a self-devised stepwise approach with a Ru catalyst in water. They confirmed that hydrogen pressure significantly influences selectivity performance. Creaser et al. [18,19], investigated the influence of support acidity on product selectivity during the PPE HDO process. They established that acidic support can improve the hydrolysis efficiency of the ether bond. Consequently, PPE serves as an effective model compound for investigating oligomers, and indeed, validating these findings through real bio-oil studies is also crucial. In terms of catalyst selection, Ru has been widely studied as an active metal for HDO, exhibiting high catalytic activity in both lignin-derived model compounds and real bio-oil [20,21]. Carrasco-Ruiz et al. [21], investigated a series of Ru-based catalysts for the HDO upgrading of bio-oil model compounds, demonstrating that well-dispersed Ru metal particles can catalyze the HDO process with both stability and efficiency. In addition, Nb_2O_5, characterized by abundant acidic sites and strong water resistance, shows significant potential as a support material in HDO processes where the bio-oil feed contains a high water content [22,23].

In this work, DFT calculations were combined with experimental studies to improve the understanding of oligomer degradation during the HDO process. PPE was selected as the model compound in this study. Initially, adsorption and reaction pathways were examined through DFT calculations. Subsequently, HDO experiments were conducted to investigate product distributions and validate the DFT simulation outcomes. Finally, bio-oil produced in a commercial fast pyrolysis plant was used for HDO experiments to corroborate the findings obtained from the model compound studies.

2. Materials and methods

2.1. DFT calculation

In this study, we performed slab model calculations utilizing the Vienna Ab-initio Simulation Package (VASP) [24,25] with the Atomic Simulation Environment (ASE) software [26]. Perdew-Burke-Ernzerhof (PBE) functional [27] with Grimme's DFT-D3 correction was applied [28]. Inner electrons were modeled using projector augmented wave (PAW) [29,30] pseudopotentials, and a cutoff energy of 400 eV. The Brillouin zone sampling was executed via a Γ-centered k-point mesh, generated employing the Monkhorst-Pack method. The Ru (0001) surface was modeled comprising of four layers, with vacuum height of 15 Å. The bottom two layers were fixed in bulk positions, while the top two layers were allowed to relax during geometry optimizations. For adsorption of PPE on Ru (0001) surface a supercell of 5 × 7 and 2 × 1 × 1 k-points were used (see supplementary information (SI), **Figure S2–4** for extensive tests). Various initial orientations were tested in order to justify the most stable one.

Geometry optimizations proceeded until the force on each atom diminished below the convergence threshold of 0.03 eV/Å, ensuring energy convergence within 10^{-6} eV. For the adsorption energy calculation, it was obtained as the Eq. (1),

$$E_{ads} = E_{total} - E_{surf} - E_{adsorbate} \quad (1)$$

where E_{total} denotes the total energy of molecule absorbate covered on a surface, E_{surf} denotes the energy of a surface, and $E_{absorbate}$ denotes the energy of molecule in vacuum.

We employed the Climbing Image Nudged Elastic Band (CINEB) [31] and dimer methods to investigate the transition states of elemental reactions. And all of the transition state structures were tested to make sure only one imaginary frequency. The reaction barrier was determined as equation 2,

$$E_{barrier} = E_{TS} - E_{IS} \quad (2)$$

where E_{TS} denotes the energy of transition state, E_{IS} denotes the energy of initial state. The thermochemistry was calculated by the package of VASPKIT [32].

2.2. Catalyst preparation and characterization

For the synthesis of Ru/Nb_2O_5, wet impregnation method was employed. Specifically, $RuCl_3{\cdot}xH_2O$ (obtained from Sigma Aldrich, USA) was used as the precursor, with a targeted loading of 5 % by weight. The metal salt was dissolved in deionized water and sonicated using a Sonorex Super RK 100 ultrasonic bath at 35 kHz for 30 minutes to ensure thorough mixing. Subsequently, amorphous Nb_2O_5 powder (sourced from CBMM, Minas Gerais, Brazil) was added to the solution to form a slurry, which was magnetically stirred for 2 h. The slurry was then evaporated at 200 rpm, 40 °C, and under a reduced pressure of 45 mbar. Then, the catalyst was dried in an oven overnight and subsequently calcined at 350 °C for 2 h. Prior to the reaction, the fresh catalyst was subjected to reduction in a tube furnace at 350 °C for 2 h under a H_2/N_2 atmosphere.

Catalyst morphology and surface elemental distribution were characterized using a Carl Zeiss DSM 982 Gemini Field Emission-SEM, equipped with secondary ion, backscattered, and transmission detectors for comprehensive surface analysis. Representative microsurface areas (1 mm^2) were subjected to elemental mapping via a Si(Li) X-ray detector (INCA Penta FET, 30 mm^2 crystal size, Oxford Instrument, UK) coupled to the SEM, providing detailed elemental composition insights. The crystalline structure was characterized using X-ray diffraction on the X'Pert PRO MPD system (PANanalytical GmbH), equipped with a Cu Kα radiation source (1.54060 Å). Data were collected across a 2θ range of 5° to 120°, employing a 0.017° step size over a duration of 1 h. The porous characteristics of Nb_2O_5 support and the synthesized catalyst through nitrogen physisorption at 77 K, utilizing a Quantachrome NovaWin instrument. Prior to measurement, the samples underwent degassing at 230 °C for 20 h. The surface area was calculated according to Brunauer–Emmett–Teller (BET) model. The acidity of the catalysts was evaluated using NH_3 Temperature-Programmed Desorption (TPD). For the measurement, 100 mg sample were placed in a quartz reactor and underwent a pretreatment of hydrogen reduction, followed by cooling to 90 °C. Subsequently, the temperature was ramped from 90 °C to 650 °C at a rate of 10 °C per minute, and this cycle was repeated five times.

2.3. Catalytic performance test

In a typical model compound HDO experiment, 0.5 g of the model compound (PPE, 97 %, acquired from VWR Chemicals), 0.5 g of the catalyst, and 50 g of the solvent (decalin, 98 %, sourced from Sigma Aldrich) were placed into a 200 ml batch reactor. The catalyst test under different temperatures was performed under 50 bar H_2 and 2-hour conditions. Prior to each reaction, the reactor was purged three times

with pure argon (Ar) to ensure complete removal of air. Throughout the reaction, the temperature was increased with a rate of 3.3 °C/min, and the mixture was stirred continuously at 600 rpm. After the reaction, the mixture was cooled to room temperature using an ice-water bath, catalyst was removed through filtration and the liquid product was then analyzed using GC–MS (Agilent 6890 N with an Agilent 5973 N mass spectrometer) for compound identification and GC-FID (HP 5890 gas chromatograph equipped with an Rxi®5Sil MS capillary column (0.25 μm × 0.25 μm × 30 m)) for quantification of each compound. The conversion and selectivity were calculated according to Eq. (3) and Eq. (4), respectively.

$$\text{Conversion}(\%) = \frac{\text{Mole of substrates consumed}}{\text{Mole of substrates fed}} \times 100\% \quad (3)$$

$$\text{Selectivity}(\%) = \frac{\text{Mole of substrates consumed to form each product}}{\text{Mole of total products}} \times 100\% \quad (4)$$

For the fast pyrolysis bio-oil HDO experiments, bio-oil was beech wood fast pyrolysis oil supplied by BTG Biomass Technology Group BV (Enschede, Netherlands). During storage, a moderate phase separation of the pyrolysis oil was observed, which was further promoted by intentional aging at 80 °C for 24 h. As a result, the upper layer, referred to as the light phase, which is rich in low and medium molecular-weight compounds. Firstly, 50 *g* of this bio-oil and 2 *g* of catalyst were introduced into a 200 mL batch reactor. The subsequent operational procedures were identical to those employed in the model compound HDO experiments. In this case, due to the more complex reactor eluent composition, centrifugation was employed for the separation of the aqueous phase, oil phase, and solid particulates. GC–MS was utilized to identify the various compounds in the oil phase, and GC (6890 Agilent, equipped with a valve switching system and two columns (Restek 57,096 Hayesep Q and Restek Molsieve 5A)) was used to identify and quantify the compounds for gas products. The contents of carbon, hydrogen, and nitrogen were determined through elemental analysis using a Leco True Spec Macro instrument (LECO Europe). The oxygen content was inferred based on the assumption that the samples consisted solely of carbon, nitrogen, hydrogen, and oxygen.

3. Results and discussion

3.1. Calculation of the adsorption energy

In Fig. 1a and 1b**,** the PPE on Ru (0001) adsorption structure is presented. The adsorption energy of PPE on Ru (0001) was found to be exceptionally high, at −4.49 eV, indicating the formation of a highly stable adsorption structure between the molecule and the surface. This is probably due to the adsorption of two aromatic rings that are known to adsorb rather strongly on the Ru surface, e.g. DFT calculations (PBE functional) of benzene adsorption on Ru (0001) have given energies between 1.40 and 1.60 eV [33–35]. Due to the high unsaturated bonds in benzene, the benzene ring of PPE is adsorbed at the most favorable site [36], thus showing that specific strong functional groups direct adsorption geometries and the corresponding energy [33]. Subsequently, charge density difference analysis was conducted to gain insights into charge distribution, as illustrated in Fig. 1c and 1d The results indicate a significant change around the two benzene rings, suggesting a robust adsorption interaction between the benzene ring and the surface. To corroborate these findings, the adsorption study of benzene on the Ru (0001) surface was examined, as demonstrated in **Figure S5**. The adsorption energy of one benzene molecule is −2.33 eV, thus about 50 % of the PPE adsorption. Note that our adsorption energies are higher due to the use of the D3 contribution, which is absent in earlier computational studies. This confirms that the adsorption energy of PPE is primarily attributed to the benzene structure.

3.2. Reaction pathway of PPE HDO

The identified reaction pathways are shown in Fig. 2. In these calculations, it is hypothesized that no C—C bond cleavage occurs during the PPE HDO process, because of the higher theoretical bond energies of C—C bonds and consistent with previous experimental research findings [37,38]. For the breaking of the C—O bond in the β-O-4 linkage, the results indicate that dehydrogenation followed by cleavage is the most probable reaction pathway. In this reaction pathway, the highest reaction barrier is the 0.59 eV of the monomer hydrogenation step. In order to investigate the reaction barrier under actual reaction conditions (250 °C and 8 MPa) as opposed to ideal conditions, thermal corrections were applied according to the experimental parameters for this specific pathway. Fig. 3 illustrates the Gibbs free energy diagram at 250 °C,

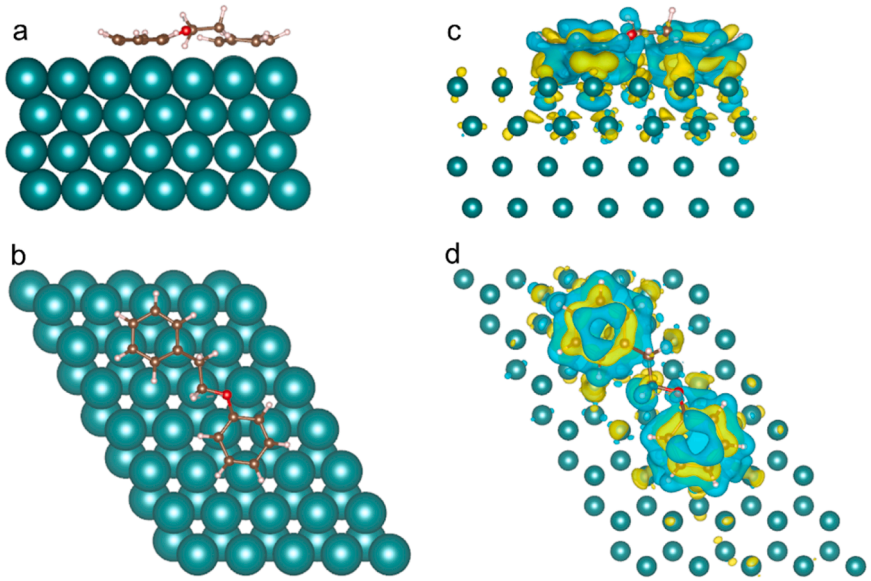

Fig. 1. The PPE on Ru (0001) adsorption structure (**a, b**) and the charge difference density plots for PPE adsorption (**c, d**). The blue-yellow distribution corresponds to charge accumulation (depletion).

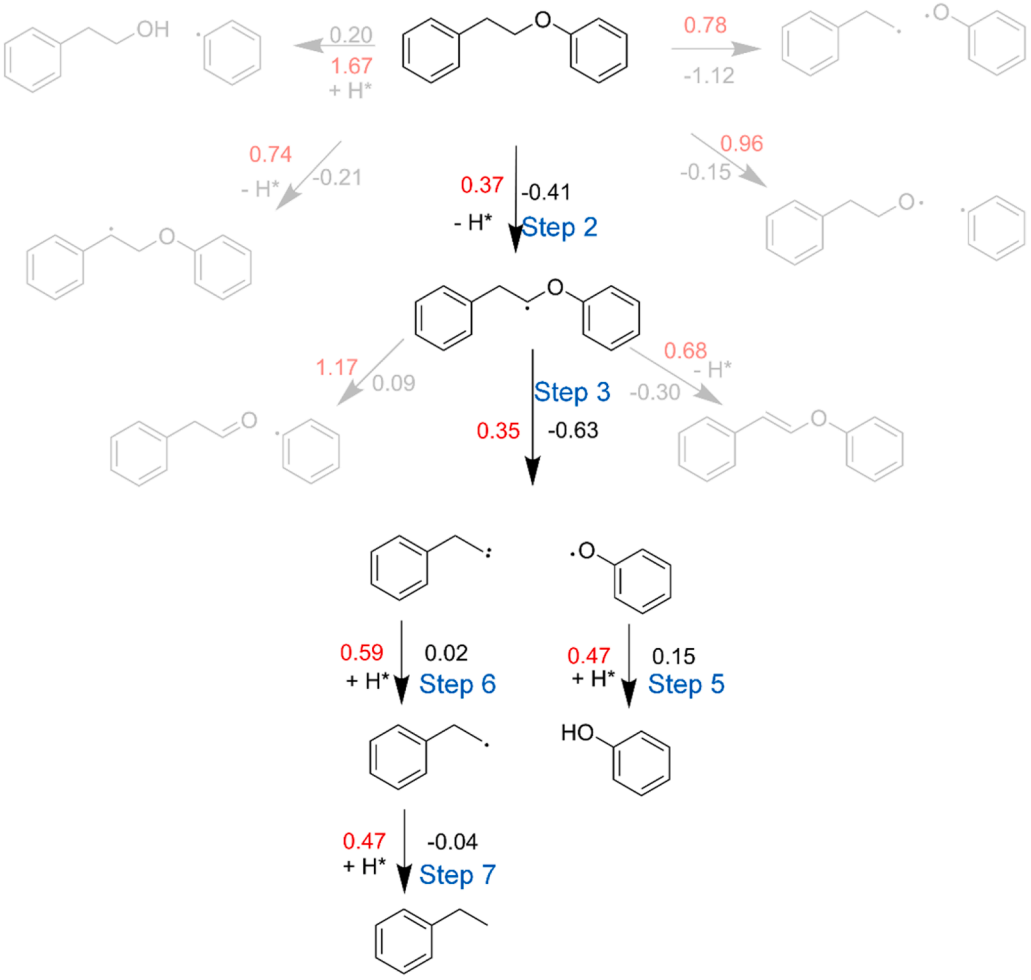

Fig. 2. Reaction pathways of PPE HDO process, red values are energy barriers, black values are reaction energy in eV, and the blue Steps correspond to the steps in Table 1.

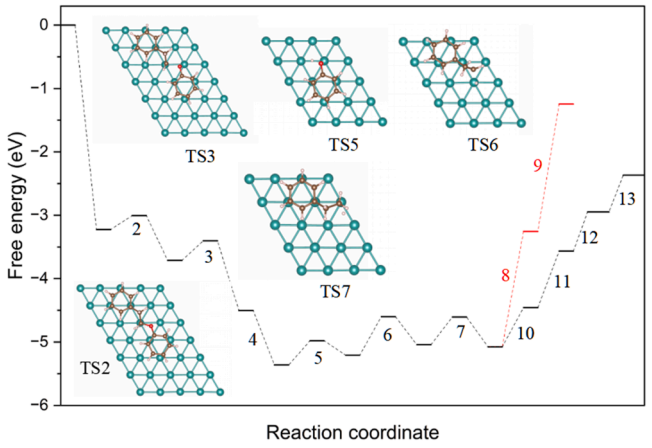

Fig. 3. Gibbs free energy diagram of PPE HDO process on Ru (0001) surface at a temperature of 250 °C. The black numbers refer to the elemental steps (see also Table 1), the 7 optimized transition states (TS) are shown as an inset. Blue values denote free energy changes during elemental reaction steps while the red values denote reaction free energy barriers.

including the transition state structures, and all of element steps are compiled in Table 1. The entire reaction pathway reveals that the reaction barrier for C—O bond cleavage step is very low, showing a value of 0.31 eV as shown in Fig. 3, step3. Additionally, the hydrogenation of

Table 1
Reaction steps corresponding Fig. 3.

	Element steps
1	$C_6H_5CH_2CH_2OC_6H_5$ (g)→ $C_6H_5CH_2CH_2OC_6H_5$*
2	$C_6H_5CH_2CH_2OC_6H_5$* → $C_6H_5CH_2CHOC_6H_5$* + H*
3	$C_6H_5CH_2CHOC_6H_5$* → $C_6H_5CH_2CH$* + *OC_6H_5
4	H_2 (g) → 2H*
5	C_6H_5O* + H* → C_6H_5OH*
6	$C_6H_5CH_2CH$* + H* → $C_6H_5CH_2CH_2$*
7	$C_6H_5CH_2CH_2$* + H*→ $C_6H_5CH_2CH_3$*
8	C_6H_5OH* → C_6H_5OH (g)
9	$C_6H_5CH_2CH_3$* → $C_6H_5CH_2CH_3$ (g)
10	C_6H_5OH* + 6H* → $C_6H_{11}OH$*
11	$C_6H_5CH_2CH_3$* + 6H* → $C_6H_{11}CH_2CH_3$*
12	$C_6H_{11}OH$* → $C_6H_{11}OH$ (g)
13	$C_6H_{11}CH_2CH_3$* → $C_6H_{11}CH_2CH_3$ (g)

monomer intermediates represents the limiting step. The desorption energies of phenol and ethylbenzene are very high, as shown in Fig. 3, steps 8 and 9. And their saturated compounds (hydrogenation of the aromatic ring) can be more easily desorbed from catalyst surface, as shown in Fig. 3 steps 12 and 13. Therefore, both molecules could potentially be further hydrogenated to saturated compounds. Overall, it can be concluded that Ru is an exceptionally potent catalyst for breaking the C—O bond with a very low energy barrier.

3.3. Catalyst characterization and HDO performance

The morphological features of Ru/Nb_2O_5 catalyst are presented in Fig. 4a, b. As it can be seen in Fig. 4a, Nb_2O_5 support is composed of numerous discrete small blocks, while Ru nanoparticles are characterized by a star shape morphology, of approximately 100–200 nm, which is sufficiently large to facilitate the exposure of the clean Ru (0001) surface. EDX mapping analysis of the sample (Fig. 4c) revealed the homogeneous distribution of Ru on Nb_2O_5 support. The Ru content, as determined from EDX mapping and presented in **Table S1**, is approximately 7.28 %. This value surpasses the expected 5 % content set during the catalyst preparation, suggesting an enrichment of Ru on the surface of the support material. To elucidate the crystalline structure of the catalyst, X-ray diffraction (XRD) analysis was conducted. The results, shown in Fig. 4d, exhibit well-defined peaks corresponding to Ru, indicating the high crystallinity of the Ru particles. The peaks at 38.38°, 42.18°, 44.01°, 58.34°, 69.41°, and 78.39° can be attributed to the hexagonal crystal structure of Ru. Regarding the Nb_2O_5 support material, its transformation to the TT-phase (pseudohexagonal) due to calcination at 380 °C typically results in the absence of significant peaks. However, an indistinct peak is observed between 20° and 30°, aligning with the findings reported by Campos Fraga et al. [39]. The N_2 physisorption results are shown in Fig. 4e and Table 2. After loading Ru onto the surface of Nb_2O_5, the catalyst exhibits a slight decrease in specific surface area, pore volume, and pore size compared to Nb_2O_5 without Ru

Table 2
N_2 physisorption results of Nb_2O_5 and Ru/Nb_2O_5.

	Surface area (m^2/g_{cat})	Pore volume (cm^3/g_{cat})	Pore diameter (nm)
Nb_2O_5	93	0.12	3.6
Ru/Nb_2O_5	88	0.11	3.5

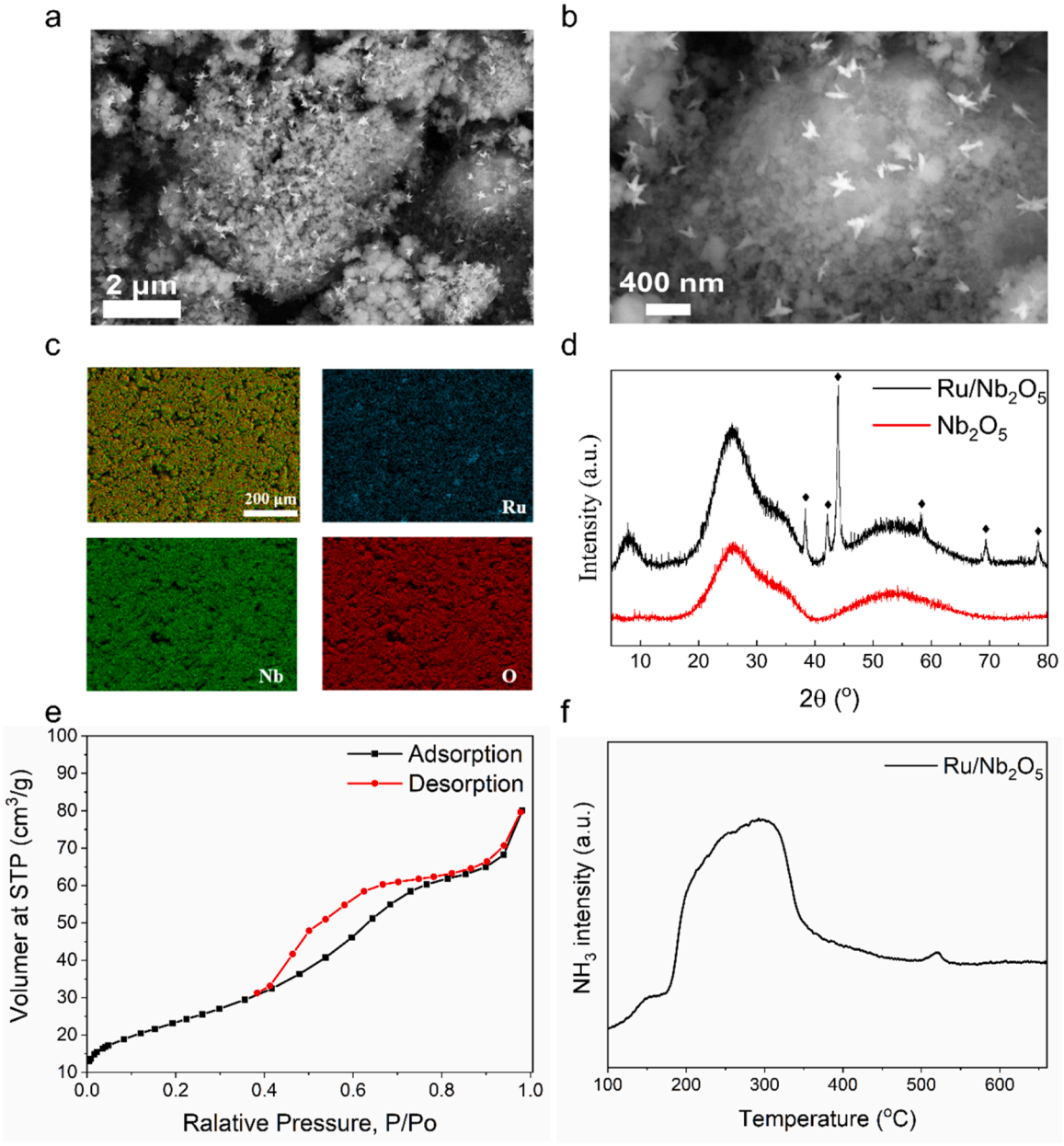

Fig. 4. SEM images of fresh Ru/Nb_2O_5 (a, b), EDX elemental mapping of Ru, Nb, O (c), XRD patterns of Ru/Nb_2O_5 (d), N_2 physisorption analysis of Ru/Nb_2O_5 (e), NH_3 TPD analysis of Ru/Nb_2O_5 (f).

loading. The results of NH_3 TPD are illustrated in Fig. 4f, wherein the acidic sites of Ru/Nb_2O_5 are predominantly concentrated in the low-temperature range of 200- 350 °C, indicating the prevalence of weak acidic sites as the primary acidic species, with an acidity value of 175.77 μmol/g.

The experimental results of PPE HDO at different temperatures are depicted in Fig. 5, where the conversion remain close to 100 % across various temperatures. At lower temperatures, the primary product of the reaction is the dimer product, mainly resulting from benzene ring hydrogenation, and the proposed formation mechanism is shown in **Figure S6**. This suggests that the Ru/ Nb_2O_5 catalyst exhibits notable hydrogenation capability and benzene ring hydrogenation efficiency even at low temperatures [40]. However, as the temperature rises, the dimer product gradually decreases, until at 250 °C, the products consist entirely of cyclohexane and ethylcyclohexane. These findings align with our DFT calculations presented in Section 3.2, which identified these products as derivatives from the hydrogenation of ethylbenzene and the HDO of phenol. Regarding the formation of hydrogenated monomers rather than arene products such as ethylbenzene, it is hypothesized that the arene products may exhibit a tendency towards strong adsorption onto the Ru surface. Supporting this hypothesis, our DFT results as illustrated in Fig. 3, indicate high desorption energies for ethylbenzene and phenol, rationalizing their further hydrogenation into the experimentally observed products like cyclohexane and ethylcyclohexane. Additionally, variations in reaction time yielded only minor changes in product distribution (as shown in **Figure S7**), implying that the catalyst's activity is sufficiently robust to achieve a high reaction rate.

3.4. Bio-oil HDO

In assessing the performance on bio-oil HDO, we utilized BTG light phase fast pyrolysis oil for testing the Ru/Nb_2O_5 catalyst. The gaseous products, collected after cooling the reactor, were immediately analyzed using GC. The results, as indicated in Table 3, demonstrate that the oxygen in bio-oil predominantly converted to CO_2 and some CO in the gas products, with negligible organic gas presence. For instance, CH_4 content was only 0.06 %. This suggests a low likelihood of direct cleavage of carbon-containing groups in bio-oil to form organic gas products, thereby avoiding carbon loss in the HDO process. The elemental analysis results are presented in Table 4, indicating a notable decrease in oxygen content. The compounds present in the oil phase-including furans, phenols, guaiacols, ketones, carboxylic acids, and esters-were identified by GC–MS in both the raw bio-oil (**Table S2**) and the upgraded bio-oil (**Table S3**). By contrasting these two data sets, we observe several notable transformations, including demethoxylation reactions of phenolic compounds, hydrogenation of furan derivatives to cyclopentanones, hydrogenation/deoxygenation of ketones to hydrocarbons, and desulfurization of sulfur-containing species. Despite the upgrading process, the bio-oil still contained a significant number of oxygen-containing compounds and many unsaturated groups. This could be attributed to the use of raw bio-oil without solvent, leading to insufficient mixing and reduced adsorption of organic compounds on the catalyst surface. Additionally, the high-water content in the raw bio-oil might have inhibited the catalytic activity, or some minor presence of inorganic cations like Na^+ or K^+. The oxygen from bio-oil which was converted into H_2O is neither part of the gas phase in Table 3 nor of the oil phase in Table S3 and was not part of this investigation.

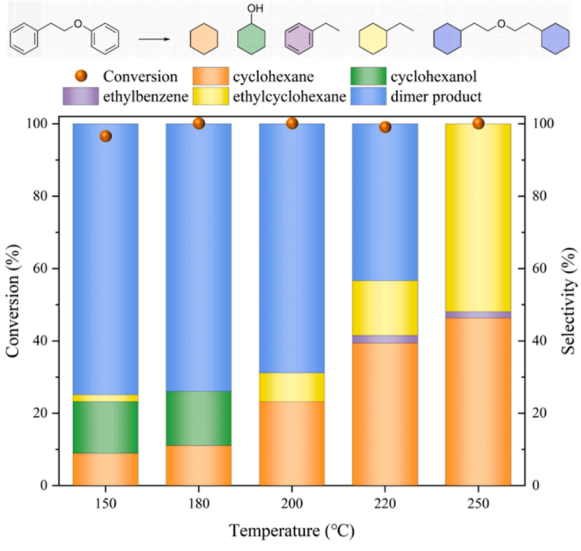

Fig. 5. Effect of temperature on PPE HDO. Condition: 0.5 g PPE, 50 g decalin, 0.5 g Ru/Nb_2O_5, 5 MPa H_2, 2 h.

Table 3
Composition of the gas phase after the reaction.

	H_2	CO_2	CO	CH_4	C_2–C_3
Content (w %)	89.19	8.38	0.71	0.06	0.04

Table 4
Element content result of crude oil and upgrade oil.

	Content (%)			
	C	H	N	O
Crude oil	42.76	7.18	2.42	47.65
Upgrade oil	63.25 ± 0.84	6.74 ± 0.09	0.29 ± 0.01	29.72 ± 0.75

4. Conclusion

In summary, the investigation of Ru catalysts in the HDO process was conducted through a combination of DFT calculations and experimental tests. The study utilized a dimer model compound, which can be regarded as a bridge between monomeric and oligomeric systems. The PPE molecule exhibited strong adsorption on the Ru (0001) surface, with the adsorption energy of PPE being nearly double that of benzene. This enhanced adsorption is attributed primarily to the 2 benzene rings in PPE, particularly when positioned at their optimal adsorption sites. In exploring the reaction pathways of PPE HDO on the Ru (0001) surface, it was observed that the energy barrier for β-O-4 linkage cleavage is notably low. And the step with the highest energy barrier is the hydrogenation of the monomeric products of the dimer cleavage. Experimentally, the Ru/Nb_2O_5 catalyst demonstrated exceptional performance in PPE HDO, achieving nearly 100 % conversion at 250 °C and 5 MPa. The main products identified were benzene, cyclohexane, and ethylcyclohexane. Furthermore, when applied to real bio-oil HDO, the Ru/Nb_2O_5 catalyst maintained a significant effect, despite the presence of oxygen-containing compounds. In conclusion, this work demonstrates that PPE, as a prototypical dimer model compound, provides a valuable link between traditional monomer studies and real bio-oil research, thereby offering insights into the effectiveness of Ru-based catalysts in HDO processes.

CRediT authorship contribution statement

Yanjun Wen: Writing – original draft, Visualization, Software, Methodology, Investigation, Conceptualization. **Foteini Zormpa:** Writing – review & editing, Methodology. **Dmitry I. Sharapa:** Writing – review & editing, Supervision, Methodology. **Felix Studt:** Writing – review & editing, Supervision. **Klaus Raffelt:** Writing – review & editing, Supervision, Methodology, Investigation. **Nicolaus Dahmen:** Writing – review & editing, Supervision.

Declaration of competing interest

The authors declare that they have no known competing financial interests or personal relationships that could have appeared to influence the work reported in this paper.

Acknowledgements

Y.W. gratefully acknowledges the financial support of the Chinese Scholarship Council for a scholarship. The authors acknowledge support by the state of Baden-Württemberg through bwHPC and the German Research Foundation (DFG) through grant no INST 40/575–1 FUGG (JUSTUS 2 cluster) and bwunicluster.

Supplementary materials

Supplementary material associated with this article can be found, in the online version, at doi:10.1016/j.mcat.2025.115134.

Data availability

Data will be made available on request.

References

[1] C. Li, X. Zhao, A. Wang, G.W. Huber, T. Zhang, Catalytic transformation of lignin for the production of chemicals and fuels, Chem. Rev. 115 (2015) 11559–11624, https://doi.org/10.1021/acs.chemrev.5b00155.
[2] E.Calcio Gaudino, G. Cravotto, M. Manzoli, S. Tabasso, Sono- and mechanochemical technologies in the catalytic conversion of biomass, Chem. Soc. Rev. 50 (2021) 1785–1812, https://doi.org/10.1039/D0CS01152E.
[3] A. Devi, A. Singh, S. Bajar, D. Pant, Z.U. Din, Ethanol from lignocellulosic biomass: an in-depth analysis of pre-treatment methods, fermentation approaches and detoxification processes, J. Environ. Chem. Eng. 9 (2021) 105798, https://doi.org/10.1016/j.jece.2021.105798.
[4] A. Molino, S. Chianese, D. Musmarra, Biomass gasification technology: the state of the art overview, J. Energy Chem. 25 (2016) 10–25, https://doi.org/10.1016/j.jechem.2015.11.005.
[5] C.C. Schmitt, R. Moreira, R.C. Neves, D. Richter, A. Funke, K. Raffelt, J.-D. Grunwaldt, N. Dahmen, From agriculture residue to upgraded product: the thermochemical conversion of sugarcane bagasse for fuel and chemical products, Fuel Process. Technol. 197 (2020) 106199, https://doi.org/10.1016/j.fuproc.2019.106199.
[6] A. Niebel, A. Funke, C. Pfitzer, N. Dahmen, N. Weih, D. Richter, B. Zimmerlin, Fast pyrolysis of wheat straw—Improvements of operational stability in 10 years of Bioliq Pilot Plant operation, Energy Fuels 35 (2021) 11333–11345, https://doi.org/10.1021/acs.energyfuels.1c00851.
[7] Y. Han, M. Gholizadeh, C.-C. Tran, S. Kaliaguine, C.-Z. Li, M. Olarte, M. Garcia-Perez, Hydrotreatment of pyrolysis bio-oil: a review, Fuel Process. Technol. 195 (2019) 106140, https://doi.org/10.1016/j.fuproc.2019.106140.
[8] I. Hita, T. Cordero-Lanzac, F.J. Garcia-Mateos, M.J. Azkoiti, J. Rodriguez-Mirasol, T. Cordero, J. Bilbao, Enhanced production of phenolics and aromatics from raw bio-oil using HZSM-5 zeolite additives for PtPd/C and NiW/C catalysts, Appl. Catal. B-Environ. 259 (2019), https://doi.org/10.1016/j.apcatb.2019.118112.
[9] J.Y. Jiang, W.T. Ding, H. Li, Promotional effect of F for Pd/HZSM-5 catalyst on selective HDO of biobased ketones, Renew. Energy 179 (2021) 1262–1270, https://doi.org/10.1016/j.renene.2021.07.065.
[10] R.Y. Shu, B.Q. Lin, J.T. Zhang, C. Wang, Z. Yang, Y. Chen, Efficient catalytic hydrodeoxygenation of phenolic compounds and bio-oil over highly dispersed Ru/TiO2, Fuel Process. Technol. 184 (2019) 12–18, https://doi.org/10.1016/j.fuproc.2018.11.004.
[11] F.F. Zormpa, A.G. Margellou, S.A. Karakoulia, E. Delli, K.S. Triantafyllidis, Hydrodeoxygenation of lignin bio-oil model compounds and surrogate mixtures over zeolite supported nickel catalysts, Catal. Today 433 (2024) 114654, https://doi.org/10.1016/j.cattod.2024.114654.
[12] W.L. Wang, X.B. Wang, Z.H. Ma, C. Duan, S.W. Liu, H.L. Yu, X.P. Li, L.P. Cai, S. Q. Shi, Y.H. Ni, Breaking the lignin conversion bottleneck for multiple products: co-production of aryl monomers and carbon nanospheres using one-step catalyst-free depolymerization, Fuel 285 (2021), https://doi.org/10.1016/j.fuel.2020.119211.
[13] W. Guan, X. Chen, H. Hu, C.-W. Tsang, J. Zhang, C.S.K. Lin, C. Liang, Catalytic hydrogenolysis of lignin β-O-4 aryl ether compound and lignin to aromatics over Rh/Nb2O5 under low H2 pressure, Fuel Process. Technol. 203 (2020) 106392, https://doi.org/10.1016/j.fuproc.2020.106392.
[14] C. Heitner, D. Dimmel, J. Schmidt, Lignin and Lignans: Advances in Chemistry, 1st ed., CRC Press, Boca Raton, 2016.
[15] Q. Li, N. López, Chirality, rigidity, and conjugation: a first-principles study of the key molecular aspects of lignin depolymerization on Ni-based catalysts, ACS Catal. 8 (2018) 4230–4240, https://doi.org/10.1021/acscatal.8b00067.
[16] J. He, D. Tang, C. Hu, Y. Luo, C.K. Kim, Z. Su, Mechanistic study on the depolymerization of typical lignin-derived oligomers catalyzed by Pd/NbOPO4, Mol. Catal. 528 (2022) 112500, https://doi.org/10.1016/j.mcat.2022.112500.
[17] Z. Luo, C. Zhao, Mechanistic insights into selective hydrodeoxygenation of lignin-derived β-O-4 linkage to aromatic hydrocarbons in water, Catal. Sci. Technol. 6 (2016) 3476–3484, https://doi.org/10.1039/C5CY01434D.
[18] M.A. Salam, P. Arora, H. Ojagh, Y.W. Cheah, L. Olsson, D. Creaser, NiMoS on alumina-USY zeolites for hydrotreating lignin dimers: effect of support acidity and cleavage of C–C bonds, Sustain. Energy Fuels 4 (2020) 149–163, https://doi.org/10.1039/C9SE00507B.
[19] M.A. Salam, Y.W. Cheah, P.H. Ho, L. Olsson, D. Creaser, Hydrotreatment of lignin dimers over NiMoS-USY: effect of silica/alumina ratio, Sustain. Energy Fuels 5 (2021) 3445–3457, https://doi.org/10.1039/D1SE00412C.
[20] E. Naranov, A. Sadovnikov, O. Arapova, T. Kuchinskaya, O. Usoltsev, A. Bugaev, K. Janssens, D. De Vos, A. Maximov, The in-situ formation of supported hydrous ruthenium oxide in aqueous phase during HDO of lignin-derived fractions, Appl. Catal. B Environ. 334 (2023) 122861, https://doi.org/10.1016/j.apcatb.2023.122861.
[21] S. Carrasco-Ruiz, S. Parrilla-Lahoz, J.L. Santos, A. Penkova, J.A. Odriozola, T. R. Reina, L. Pastor-Perez, Water-assisted HDO of biomass model compounds enabled by Ru-based catalysts, Fuel Process. Technol. 249 (2023) 107860, https://doi.org/10.1016/j.fuproc.2023.107860.
[22] H. Xu, H. Li, Regulating the crystal phase of Pd/Nb2O5 for vanillin selective HDO at room temperature, J. Catal. 423 (2023) 105–117, https://doi.org/10.1016/j.jcat.2023.04.010.
[23] K.L. Patle, P. Pardhi, S. Pantawane, D.T. Sarve, Jayant. Ekhe, K.L. Wasewar, Nb_2O_5 supported metal-based heterogeneous catalysts for hydrodeoxygenation (HDO) of lignin-derived molecules: a powerful tool for generating fuel-additive products including hydrocarbons, Catal. Rev. (2025) 1–53, https://doi.org/10.1080/01614940.2025.2453713.
[24] G. Kresse, J. Furthmüller, Efficiency of ab-initio total energy calculations for metals and semiconductors using a plane-wave basis set, Comput. Mater. Sci. 6 (1996) 15–50, https://doi.org/10.1016/0927-0256(96)00008-0.
[25] G. Kresse, J. Furthmüller, Efficient iterative schemes for ab initio total-energy calculations using a plane-wave basis set, Phys. Rev. B 54 (1996) 11169–11186, https://doi.org/10.1103/PhysRevB.54.11169.
[26] S.R. Bahn, K.W. Jacobsen, An object-oriented scripting interface to a legacy electronic structure code, Comput. Sci. Eng. 4 (2002) 56–66, https://doi.org/10.1109/5992.998641.
[27] J.P. Perdew, K. Burke, M. Ernzerhof, Generalized gradient approximation made simple, Phys. Rev. Lett. 77 (1996) 3865–3868, https://doi.org/10.1103/PhysRevLett.77.3865.
[28] S. Grimme, J. Antony, S. Ehrlich, H. Krieg, A consistent and accurate *ab initio* parametrization of density functional dispersion correction (DFT-D) for the 94 elements H-Pu, J. Chem. Phys. 132 (2010) 154104, https://doi.org/10.1063/1.3382344.
[29] P.E. Blöchl, Projector augmented-wave method, Phys. Rev. B 50 (1994) 17953–17979, https://doi.org/10.1103/PhysRevB.50.17953.
[30] G. Kresse, D. Joubert, From ultrasoft pseudopotentials to the projector augmented-wave method, Phys. Rev. B 59 (1999) 1758–1775, https://doi.org/10.1103/PhysRevB.59.1758.
[31] G. Henkelman, B.P. Uberuaga, H. Jónsson, A climbing image nudged elastic band method for finding saddle points and minimum energy paths, J. Chem. Phys. 113 (2000) 9901–9904, https://doi.org/10.1063/1.1329672.
[32] V. Wang, N. Xu, J.-C. Liu, G. Tang, W.-T. Geng, VASPKIT: a user-friendly interface facilitating high-throughput computing and analysis using VASP code, Comput. Phys. Commun. 267 (2021) 108033, https://doi.org/10.1016/j.cpc.2021.108033.
[33] C.C. Chiu, A. Genest, A. Borgna, N. Rosch, Hydrodeoxygenation of guaiacol over Ru(0001): a DFT study, Acs Catal. 4 (2014) 4178–4188, https://doi.org/10.1021/cs500911j.
[34] C. Fan, Y.-A. Zhu, X.-G. Zhou, Z.-P. Liu, Catalytic hydrogenation of benzene to cyclohexene on Ru(0001) from density functional theory investigations☆, Catal. Today 160 (2011) 234–241, https://doi.org/10.1016/j.cattod.2010.03.075.
[35] Y. Xia, C. Fan, Z.-L. Zhou, Y.-A. Zhu, X.-G. Zhou, Effect of Zn on the selectivity of Ru in benzene partial hydrogenation from density functional theory investigations, J. Mol. Catal. Chem. 370 (2013) 44–49, https://doi.org/10.1016/j.molcata.2012.12.014.
[36] Ab initio DFT studies of adsorption characteristics of benzene on close-packed surfaces of transition metals, Comput. Mater. Sci. 137 (2017) 10–19, https://doi.org/10.1016/j.commatsci.2017.05.019.
[37] A. Bjelic, B. Likozar, M. Grilc, Scaling of lignin monomer hydrogenation, hydrodeoxygenation and hydrocracking reaction micro-kinetics over solid metal/acid catalysts to aromatic oligomers, Chem. Eng. J. 399 (2020), https://doi.org/10.1016/j.cej.2020.125712.
[38] H.-B. Gao, L.-L. Qiu, F.-P. Wu, J. Xiao, Y.-P. Zhao, J. Liang, Y.-H. Bai, F.-J. Liu, J.-P. Cao, Highly efficient catalytic hydrogenolysis of lignin model compounds over hydrotalcite-derived Ni/Al2O3 catalysts, Fuel 337 (2023) 127196, https://doi.org/10.1016/j.fuel.2022.127196.
[39] M.M. Campos Fraga, J. Vogt, B. Lacerda de Oliveira Campos, C.C. Schmitt, K. Raffelt, N. Dahmen, Investigation of Nb2O5 and its polymorphs as catalyst supports for pyrolysis oil upgrading through hydrodeoxygenation, Energy Fuels 37 (2023) 10474–10492, https://doi.org/10.1021/acs.energyfuels.3c01152.
[40] L. Jiang, Y. Dong, G. Zhou, R. Li, D. He, Promoting the performances of TiO2 submicrosphere-embedded Ru nanoparticles in benzene selective hydrogenation by morphology manipulation, Ind. Eng. Chem. Res. 59 (2020) 1083–1092, https://doi.org/10.1021/acs.iecr.9b05215.